Unmanned Systems, Vol. 5, No. 3 (2017) 131–139
© World Scientific Publishing Company
DOI: 10.1142/S2301385017400015

UNMANNED SYSTEMS
http://www.worldscientific.com/worldscinet/us

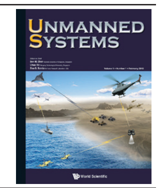

UKF–Based LQR Control of a Manipulating Unmanned Aerial Vehicle

Hossein Bonyan Khamseh*, Farrokh Janabi-Sharifi

Department of Mechanical and Industrial Engineering, Ryerson University, Toronto, Canada

Robotics, Mechatronics and Automation Laboratory (RMAL), Ryerson University, Toronto, Canada

In this paper, modeling, control and state estimation of a manipulating unmanned aerial vehicle (UAV) consisting of a quadcopter equipped with a two degree-of-freedom robotic manipulator is discussed. In the first step, Euler–Lagrange approach is adopted to model the coupled dynamics of the quadcopter and its robotic manipulator. Having linearized the obtained model, a linear quadratic regulator is designed to achieve simultaneous control of the quadcopter and the manipulator. Finally, a UKF-based algorithm is employed to obtain state estimation of the system. For a case study, simulation results are presented to verify feasibility of the proposed approach.

Keywords: Aerial manipulation; linear quadratic regulator; unscented Kalman filter; state estimation.

1. Introduction

In recent years, a significant growth in Unmanned Aerial Vehicle (UAV) industry has been realized. To this date, UAVs have been used in applications such as remote sensing of agricultural products [1], forest fire monitoring [2], search and rescue [3], transmission line inspection [4], border monitoring [5], and hobby activities. An important common element in the mentioned applications is that the UAV is employed to sense, monitor and "see" the environment, but physical interaction with the environment is strictly avoided. To that end, UAVs tend not to fly in close vicinity of walls, structures and also the ground. However, in the last few years, researchers have begun examining applications in which the UAV is required to perform perching, grasping, and manipulation [6–9]. This new area of research, usually known as aerial manipulation, encourages physical interaction of the UAV with its surrounding environment and enables UAVs to carry out a whole new set of missions. The dynamics of an aerial manipulation system, called Manipulating Unmanned Aerial Vehicle (MUAV) hereafter [10], is complex, due to inherent couplings and nonlinearities of the system. In the current literature, there are two main methods for dynamic modeling of MUAVs, namely Recursive Newton–Euler (RNE) approach and Euler–Lagrange approach [10, 11]. While both of the mentioned methods result in identical equations of motion, the former is more convenient for actual implementation whereas the latter is better suited for the study of dynamic properties and analytical investigation. In this paper, Euler–Lagrange approach is adopted to obtain coupled nonlinear dynamic model of a MUAV. Having linearized the obtained dynamic model, control design of the system is carried out. Regarding the control of MUAVs, two main categories can be identified in the present literature [12]. In the first category, known as decoupled approach, separate controllers for the UAV and the manipulator are developed [13, 14] whereas in the second category, known as coupled approach, control of a unified MUAV system is considered [15, 16]. Various approaches adopted in each category and their associated advantages and shortcomings are presented in Table 1.

In this paper, LQR scheme is used to design a coupled controller that enables simultaneous control of a quadcopter UAV and its 2-Degree-of-Freedom (DoF) manipulator. LQR is a popular control scheme in quadcopter control due to its optimal performance for given weight matrices and its easy implementation [10, 22–24]. As an example, in [22], the authors employed LQR scheme to enable a quadcopter

Received 3 November 2016; Revised 9 May 2017; Accepted 10 May 2017; Published 21 July 2017. This paper was accepted for publication in the Special issue on Aerial Robotics: Success Stories of Today and Hopes of Tomorrow. Guest Editors: Farrokh Janabi Sharifi, Youmin Zhang, Hossein Bonyan Khamseh and Howard Li.
Email Addresses: *hbonyan@ryerson.ca

Table 1. Control strategies in MUAV applications.

MUAV control	Control algorithms	Advantages	Disadvantages
Decoupled	*UAV control algorithm*: Various simple and gain–scheduling Proportional–Derivative (PD) and Proportional–Derivative–Integral (PID) [13, 17, 18] feedback linearization [15], backstepping [19] and adaptive control [16, 17] *Manipulator control algorithm*: Independent joint control (PID, PID + gravity compensation) [10, 13]	Complex model of MUAV is not required. A wealth of literature is available for UAV control (similarly for manipulator control). It is computationally less expensive.	It usually requires that UAV and manipulator are not actuated simultaneously. Relatively less accurate control
Coupled	Feedback linearization [20], impedance control [11], nonlinear backstepping [21], Linear Quadratic Regulator (LQR) [16], and model-predictive control [15]	UAV and manipulator are actuated together and therefore less time is required to accomplish a given scenario. More accurate control can be achieved.	Complex model of MUAV is required. It is computationally expensive.

to follow a given time-varying reference trajectory. Also, in [24], gain scheduling (switching) was used to improve the performance of standard LQR in quadcopter trajectory tracking. Regarding the area of aerial manipulation, in [16], LQR was used to control a small helicopter carrying a 1-DoF revolute–joint robotic arm. The findings of that work reveal that LQR controller can stabilize a small helicopter and its 1-DoF manipulator near the trim point, with acceptable performance. However, the drawback is that stabilization region of LQR controller was found to be very limited. Here, we extend the design of LQR controller to a MUAV consisting of a quadcopter and a manipulator of 2–DoF.

State estimation of MUAVs has been left largely intact to this date. Regarding the state estimation problem, Unscented Kalman Filter (UKF) is a relatively new technique that effectively avoids the linearization step of Extended Kalman Filter (EKF). The main idea behind UKF is that a Gaussian distribution can be approximated relatively easily whereas approximating an arbitrary nonlinear function is more difficult [25]. It has been shown that UKF outperforms EKF in most cases, especially for highly nonlinear process and/or measurement models [25–28]. Contrary to EKF, derivation of Jacobian matrices is not necessary in UKF.

For MUAVs, this can be beneficial as the derivation of Jacobian matrices is impractical and therefore possible implementation difficulties are avoided [26]. Instead of directly linearizing the nonlinear process and/or measurement models, UKF uses a deterministic sampling method to generate a minimal number of sigma points that capture mean and covariance estimates. The sample points are then propagated through the nonlinear process/measurement models and the mean and covariance of the estimate are numerically recovered. It can be theoretically shown that UKF accuracy is comparable to third-order Taylor series expansion, for any nonlinearity [25]. As an example, for the problem of spacecraft localization, performance of EKF was compared to UKF in [27]. For two sample missions of Earth–Moon transfer and geostationary orbit rising, it was demonstrated that UKF offers better performance in terms of localization accuracy and consistency of the estimates. Also, in [28], three-axis attitude determination of a UAV was considered. In that work, the authors found that UKF robustness to noise is much better than EKF and concluded that it is a better alternative, compared to conventional EKF. Here, performance of a UKF-based algorithm for state estimation of a MUAV is examined.

The rest of this paper is as follows. In Sec. 2, Euler–Lagrange formulation is used to obtain the dynamic model of the MUAV. In Sec. 3, design of LQR control law for simultaneous control of the quadcopter and its manipulator is studied. UKF-based state estimation of the MUAV is discussed in Sec. 4. Simulation results and conclusions are presented in Secs. 5 and 6, respectively.

2. Kinematic and Dynamic Modelling of a Quadcopter–Based MUAV

In this section, kinematic equations of a MUAV are presented. For that purpose, the MUAV shown in Fig. 1 is considered.

Here, let $F_I = \{X_I, Y_I, Z_I\}$ with the origin O_I and $F_B = \{X_B, Y_B, Z_B\}$ with the origin O_B be the inertial frame and body frame, respectively. Also, n_M is the number of

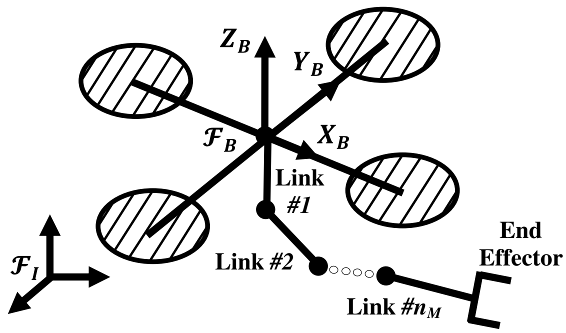

Fig. 1. Schematic view of a MUAV.

manipulator degrees of freedom. Let $\boldsymbol{p}_b = [X \quad Y \quad Z]^T$ denotes position of the F_B in the inertial frame and quadcopter attitude is represented by $\boldsymbol{\Phi}_b = [\varphi \quad \theta \quad \psi]^T$, where φ, θ and ψ are the roll, pitch and yaw angles. Therefore, one can write:

$$\begin{cases} \dot{X} = v_X, \\ \dot{Y} = v_Y, \\ \dot{Z} = v_Z, \end{cases} \tag{1}$$

$$\begin{bmatrix} \dot{\varphi} \\ \dot{\theta} \\ \dot{\psi} \end{bmatrix} = \begin{bmatrix} 1 & s_\varphi t_\theta & c_\varphi t_\theta \\ 0 & c_\varphi & -s_\varphi \\ 0 & s_\varphi / c_\theta & c_\varphi / c_\theta \end{bmatrix} \begin{bmatrix} p \\ q \\ r \end{bmatrix}, \tag{2}$$

or more compactly:

$$\dot{\boldsymbol{\Phi}}_b = \boldsymbol{T}^{-1} \boldsymbol{\omega}_b, \tag{3}$$

where $s_{(\alpha)}$, $c_{(\alpha)}$ and $t_{(\alpha)}$ denote trigonometric sine, cosine and tangent functions of the variable α. Also, p, q and r denote the three components of the angular velocity vector, i.e. $\boldsymbol{\omega}_b = [p, q, r]^T$. The corresponding rotation matrix from the body frame to the inertia frame is given by:

$$\boldsymbol{R}_b = \begin{bmatrix} c_\psi c_\theta & -s_\psi c_\varphi + c_\psi s_\theta s_\varphi & s_\psi s_\varphi + c_\psi s_\theta c_\varphi \\ s_\psi c_\theta & c_\psi c_\varphi + s_\psi s_\theta s_\varphi & -c_\psi s_\varphi + s_\psi s_\theta c_\varphi \\ -s_\theta & c_\theta s_\varphi & c_\theta c_\varphi \end{bmatrix}. \tag{4}$$

What is more, Eq. (2) can be written in the body frame as:

$$\boldsymbol{\omega}_b^b = \boldsymbol{R}_b^T \boldsymbol{\omega}_b = \boldsymbol{R}_b^T \boldsymbol{T} \dot{\boldsymbol{\Phi}}_b = \boldsymbol{Q} \dot{\boldsymbol{\Phi}}_b. \tag{5}$$

In order to obtain the kinematic equations of the end-effector, it is helpful to consider a frame at the center-of-mass of each link, where the frame coordinates coincide with link principal axes of inertia. Denoting the position of the frame on link i by $\boldsymbol{p}_{l_i}$, one can write:

$$\boldsymbol{p}_{l_i} = \boldsymbol{p}_b + \boldsymbol{R}_b \boldsymbol{p}_{bl_i}^b, \tag{6}$$

where $\boldsymbol{p}_{bl_i}^b$ denotes the vector position of the frame on link i with respect to $\mathcal{F}_{\mathrm{B}}$, expressed in the $\mathcal{F}_{\mathrm{B}}$. As a result, $\dot{\boldsymbol{p}}_{bl_i}^b$ is given by [29]:

$$\dot{\boldsymbol{p}}_{bl_i}^b = \boldsymbol{J}_{P1}^{(l_i)} \dot{q}_1 + \cdots + \boldsymbol{J}_{Pi}^{(l_i)} \dot{q}_i = \boldsymbol{J}_P^{(l_i)} \dot{\boldsymbol{q}}, \tag{7}$$

where $\boldsymbol{J}_P^{(l_i)}$ represents contribution of the manipulator Jacobian to linear velocity up to link i and $\boldsymbol{q} = [q_1 \quad \ldots \quad q_{n_M}]^T$ denotes the robotic manipulator joint variables. Also, denoting the angular velocity of the frame on link i with respect to the body frame by $\boldsymbol{\omega}_{l_i}^b$, one can write:

$$\boldsymbol{\omega}_{l_i}^b = \boldsymbol{J}_{O1}^{(l_i)} \dot{q}_1 + \cdots + \boldsymbol{J}_{Oi}^{(l_i)} \dot{q}_i = \boldsymbol{J}_O^{(l_i)} \dot{\boldsymbol{q}}. \tag{8}$$

Similarly, $\boldsymbol{J}_O^{(l_i)}$ represents contribution of the manipulator Jacobian to angular velocity up to link i. Therefore, one can write:

$$\dot{\boldsymbol{p}}_{l_i} = \dot{\boldsymbol{p}}_b - S(\boldsymbol{R}_b \boldsymbol{p}_{bl_i}^b) \boldsymbol{\omega}_b + \boldsymbol{R}_b \boldsymbol{J}_P^{(l_i)} \dot{\boldsymbol{q}}, \tag{9}$$

where $S(\cdot)$ denotes the skew-symmetric matrix operator. Similarly, the kinematic angular velocity equation is obtained:

$$\boldsymbol{\omega}_{l_i} = \boldsymbol{\omega}_b + \boldsymbol{R}_b \boldsymbol{J}_O^{(l_i)} \dot{\boldsymbol{q}}. \tag{10}$$

Having obtained the kinematic equation, the popular so-called Euler–Lagrange formulation is adopted to obtain the dynamic equations of a MUAV [11]. To that end, one needs to formulate the system Lagrangian $\mathcal{L} = \mathcal{K} - \mathcal{U}$ where $\mathcal{K}$ and $\mathcal{U}$ represent the system kinetic and potential energy, respectively. Having calculated L, Lagrange equations are given by:

$$\frac{d}{dt} \frac{\partial \mathcal{L}}{\partial \dot{\xi}_i} - \frac{\partial \mathcal{L}}{\partial \xi_i} = u_{\mathrm{MUAV},i}, \tag{11}$$

where ξ_i is the ith element of the generalized vector $\boldsymbol{\xi} = [\boldsymbol{p}_b^T \quad \boldsymbol{\Phi}_b^T \quad \boldsymbol{q}^T]^T$ and $\boldsymbol{u}_{\mathrm{MUAV}} \in \mathbb{R}^{(4+n_M)}$ is the ith system input. MUAV total kinetic energy is given by:

$$\mathcal{K} = \mathcal{K}_b + \sum_{i=1}^{n_M} \mathcal{K}_{l_i}, \tag{12}$$

where $\mathcal{K}_b$ and $\mathcal{K}_{l_i}$ denote the kinetic energy of the quadcopter and link i, respectively. Kinetic energy of the quadcopter, in turn, is given by:

$$\mathcal{K}_b = \frac{1}{2} m_b \dot{\boldsymbol{p}}_b^T \dot{\boldsymbol{p}}_b + \frac{1}{2} \dot{\boldsymbol{\Phi}}_b^T \boldsymbol{Q}^T \boldsymbol{H}_b \boldsymbol{Q} \dot{\boldsymbol{\Phi}}_b, \tag{13}$$

where m_b and $\boldsymbol{H}_b$ are the mass and inertia matrix of the UAV, respectively. Also, kinetic energy of link i is given by:

$$\mathcal{K}_{l_i} = \frac{1}{2} m_{l_i} \dot{\boldsymbol{p}}_{l_i}^T \dot{\boldsymbol{p}}_{l_i} + \frac{1}{2} \boldsymbol{\omega}_{l_i}^T \boldsymbol{R}_b \boldsymbol{R}_{l_i}^b \boldsymbol{H}_{l_i} \boldsymbol{R}_b^{l_i} \boldsymbol{R}_b^T \boldsymbol{\omega}_{l_i}, \tag{14}$$

where $\boldsymbol{R}_{l_i}^b$ is the rotation matrix from the frame on link i to the body frame. Also, m_{l_i} and $\boldsymbol{H}_{l_i}$ are the mass and inertia matrix of link i, respectively. As a result, the total kinetic energy can be expressed in compact form as:

$$\mathcal{K} = \frac{1}{2}\dot{\boldsymbol{\xi}}^T\boldsymbol{B}\dot{\boldsymbol{\xi}}, \tag{15}$$

where $\boldsymbol{B} \in \mathbb{R}^{(6+n_M)\times(6+n_M)}$ is the symmetric and positive definite inertia matrix whose elements are given by [11]:

$$\boldsymbol{B}_{11} = \left(\boldsymbol{m}_b + \sum_{i=1}^{n_M} m_{l_i}\right)\boldsymbol{I}_3, \tag{16}$$

$$\boldsymbol{B}_{22} = \boldsymbol{Q}^T\boldsymbol{H}_b\boldsymbol{Q} + \sum_{i=1}^{n_M}(m_{l_i}\boldsymbol{T}^T S(\boldsymbol{R}_b\boldsymbol{p}^b_{bl_i})^T S(\boldsymbol{R}_b\boldsymbol{p}^b_{bl_i})\boldsymbol{T} + \boldsymbol{Q}^T\boldsymbol{R}^b_{l_i}\boldsymbol{H}_{l_i}\boldsymbol{R}^{l_i}_b\boldsymbol{Q}), \tag{17}$$

$$\boldsymbol{B}_{33} = \sum_{i=1}^{n_M}(m_{l_i}(\boldsymbol{J}^{(l_i)}_P)^T\boldsymbol{J}^{(l_i)}_P + (\boldsymbol{J}^{(l_i)}_O)^T\boldsymbol{R}^b_{l_i}\boldsymbol{H}_{l_i}\boldsymbol{R}^{l_i}_b\boldsymbol{J}^{(l_i)}_O), \tag{18}$$

$$\boldsymbol{B}_{12} = \boldsymbol{B}^T_{21} = -\sum_{i=1}^{n_M}(m_{l_i}(\boldsymbol{R}_b\boldsymbol{p}^b_{bl_i})\boldsymbol{T}), \tag{19}$$

$$\boldsymbol{B}_{13} = \boldsymbol{B}^T_{31} = \sum_{i=1}^{n_M}(m_{l_i}\boldsymbol{R}_b\boldsymbol{J}^{(l_i)}_P), \tag{20}$$

$$\boldsymbol{B}_{23} = \boldsymbol{B}^T_{32} = \sum_{i=1}^{n_M}(\boldsymbol{Q}^T\boldsymbol{R}^b_{l_i}\boldsymbol{H}_{l_i}\boldsymbol{R}^{l_i}_b\boldsymbol{J}^{(l_i)}_O - m_{l_i}\boldsymbol{T}^T S(\boldsymbol{R}_b\boldsymbol{p}^b_{bl_i})^T\boldsymbol{R}_b\boldsymbol{J}^{(l_i)}_P), \tag{21}$$

where $\boldsymbol{I}_\alpha$ denotes the $(\alpha \times \alpha)$ identity matrix. The potential energy of the system can be written as:

$$\mathcal{U} = \mathcal{U}_b + \sum_{i=1}^{n_M}\mathcal{U}_{l_i}, \tag{22}$$

where $\mathcal{U}_b$ and $\mathcal{U}_{l_i}$ are the potential energy of the quadcopter and that of link i, respectively. The quadcopter potential energy is given by:

$$\mathcal{U}_b = -m_b g\boldsymbol{e}^T_3\boldsymbol{p}_b, \tag{23}$$

where $\boldsymbol{e}_3 = [0 \quad 0 \quad 1]^T$ if the gravity acts along the opposite direction of Z_I. The potential energy of link i is given by:

$$\mathcal{U}_{l_i} = -m_{l_i}g\boldsymbol{e}^T_3(\boldsymbol{p}_b + \boldsymbol{R}_b\boldsymbol{p}^b_{bl_i}). \tag{24}$$

Therefore, the total potential energy of the MUAV is given by:

$$\mathcal{U} = -m_b g\boldsymbol{e}^T_3\boldsymbol{p}_b - g\sum_{i=1}^{n_M}[m_{l_i}\boldsymbol{e}^T_3(\boldsymbol{p}_b + \boldsymbol{R}_b\boldsymbol{p}^b_{bl_i})]. \tag{25}$$

Having obtained the MUAV total kinetic and potential energy, one can use Eq. (11) to obtain the MUAV dynamic equations of motion as:

$$\boldsymbol{B}(\boldsymbol{\xi})\ddot{\boldsymbol{\xi}} + \boldsymbol{C}(\boldsymbol{\xi},\dot{\boldsymbol{\xi}})\dot{\boldsymbol{\xi}} + \boldsymbol{g}(\boldsymbol{\xi}) = \boldsymbol{u}_{\text{MUAV}}. \tag{26}$$

In Eq. (26), $\boldsymbol{C}$ is the centrifugal and Coriolis matrix and $\boldsymbol{g}$ is the gravitational vector. The input $\boldsymbol{u}_{\text{MUAV}} \in \mathbb{R}^{(4+n_M)}$ is given by [11]:

$$\boldsymbol{u}_{\text{MUAV}} = \bar{\boldsymbol{R}}\boldsymbol{N}\boldsymbol{F}, \tag{27}$$

in which: $\boldsymbol{F} = [\boldsymbol{T}^T_b \quad \boldsymbol{\tau}^T]^T$, where $\boldsymbol{T}_b \in \mathbb{R}^4$ is the input vector of forces from quadcopter and $\boldsymbol{\tau} \in \mathbb{R}^{n_M}$ is the input vector of torques from manipulator joints. Also, $\boldsymbol{N} = \text{diag}(\boldsymbol{\Omega}, \boldsymbol{I}_{n_M})$ where I_{n_M} is the identity matrix of proper size and $\boldsymbol{\Omega}$ is given by [11]:

$$\boldsymbol{\Omega} = \begin{bmatrix} 0 & 0 & 0 & 0 \\ 0 & 0 & 0 & 0 \\ 1 & 1 & 1 & 1 \\ 0 & -l & 0 & l \\ -l & 0 & l & 0 \\ -d/b & d/b & -d/b & d/b \end{bmatrix}, \tag{28}$$

where l is the distance from a motor to quadcopter geometric center and b and d are drag and lift coefficient, respectively. Finally, in Eq. (27), $\bar{\boldsymbol{R}} = \text{diag}(\boldsymbol{R}_b, \boldsymbol{Q}^T, \boldsymbol{I}_{n_M})$. Next, LQR scheme is employed to design the input such that simultaneous control of the UAV and its robotic manipulator is achieved.

3. LQR Control of a Quadcopter-Based MUAV

In order to design a LQR controller, the following cost function over infinite horizon is considered [30]:

$$J(\boldsymbol{u}) = \int_0^\infty(\boldsymbol{x}^T\boldsymbol{Q}_{\text{LQR}}\boldsymbol{x} + \boldsymbol{u}^T\boldsymbol{R}_{\text{LQR}}\boldsymbol{u})dt, \tag{29}$$

in which $\boldsymbol{Q}_{\text{LQR}} \in \mathbb{R}^{(12+2*n_M)\times(12+2*n_M)}$ and $\boldsymbol{R}_{LQR} \in \mathbb{R}^{(4+n_M)\times(4+n_M)}$ are positive definite weight matrices to penalize the deviation from the reference trajectory and the magnitude of the control signal, respectively. The above cost function can be minimized by state feedback law of the form:

$$\boldsymbol{u} = -\boldsymbol{K}(\boldsymbol{x} - \boldsymbol{x}^*), \tag{30}$$

where $\boldsymbol{x}^*$ is the desired set point and the optimal gain $\boldsymbol{K}$ is obtained from:

$$\boldsymbol{K} = \boldsymbol{R}^{-1}_{\text{LQR}}\boldsymbol{B}^T\boldsymbol{P}, \tag{31}$$

and $\boldsymbol{P}$ in turn is obtained from the following Algebraic Riccati Equation (ARE) [30]:

$$\boldsymbol{A}^T\boldsymbol{P} + \boldsymbol{P}\boldsymbol{A} - \boldsymbol{P}\boldsymbol{B}\boldsymbol{R}^{-1}\boldsymbol{B}^T\boldsymbol{P} + \boldsymbol{Q}_{\text{LQR}} = \boldsymbol{0}. \tag{32}$$

The positive definite matrix $\boldsymbol{Q}_{\text{LQR}}$ can be chosen to be diagonal. If one increases the entries of $\boldsymbol{Q}_{\text{LQR}}$, the deviation from the reference trajectory will be heavily penalized and the states rapidly converge to the desired values, i.e. high control gains [30]. The positive definite matrix $\boldsymbol{R}_{\mathrm{LQR}}$ can also be chosen to be diagonal. In that case, if one increases the entries of $\boldsymbol{R}_{\mathrm{LQR}}$, the magnitude of the control signal will be heavily penalized and the control gains will be small. Thus, small values in the entries of $\boldsymbol{R}_{\mathrm{LQR}}$ will result in slower system response and control laws with relatively small magnitude [30]. Finally, finite (nonzero) steady state error is an expected shortcoming in the performance of the proposed approach. An immediate solution in this case is to add integral action to the LQR scheme, known as LQR–I hereafter, such that steady state error is eliminated [10].

4. UKF-Based State Estimation of a Quadcopter-Based MUAV

Unscented Kalman Filter (UKF) is a relatively new technique to avoid the linearization step of EKF. In UKF, a deterministic sampling technique i.e. unscented transform is utilized to generate a minimal set of sample points from the state *priori* mean and covariance. Then, these sampled points are propagated through the nonlinear process model and *posterior* mean and covariance are numerically recovered [26, 31]. The discretized kinematic and dynamic equations of a MUAV and the observation model can be written in compact form as:

$$\boldsymbol{x}_k = \boldsymbol{f}(\boldsymbol{x}_{k-1}, \boldsymbol{u}_{k-1}) + \boldsymbol{w}_k, \tag{33}$$

$$\boldsymbol{y}_k = \boldsymbol{H}\boldsymbol{x}_k + \boldsymbol{v}_k, \tag{34}$$

where $\boldsymbol{x} = [\boldsymbol{\xi}^T \quad \dot{\boldsymbol{\xi}}^T]^T$, y is the observation vector, and $\boldsymbol{w}_k$ and $\boldsymbol{v}_k$ are the state transition and observation noise with zero mean Gaussian distribution and covariance $\boldsymbol{Q}_k^*$ and $\boldsymbol{R}_k^*$, respectively. In our problem, the measurement observation vector consists of $\boldsymbol{p_b}, \psi$, and $\boldsymbol{q}$ and therefore $\boldsymbol{H} \in \mathbb{R}^{(4+n_M)\times(12+2*n_M)}$ is a constant matrix. Time-update equations of the UKF algorithm described in [26, 32] utilizes $2n$ sigma points to propagate the states whereas our algorithm is similar to [28, 33, 34] in which $2n+1$ weighted sigma points are generated:

$$\begin{cases} \boldsymbol{\chi}^0_{k-1|k-1} = \hat{\boldsymbol{x}}_{k-1|k-1}, \\ \boldsymbol{\chi}^i_{k-1|k-1} = \hat{\boldsymbol{x}}_{k-1|k-1} + \left(\sqrt{(n+\lambda)\boldsymbol{P}_{k-1|k-1}}\right)_i, \\ \boldsymbol{\chi}^{i+n}_{k-1|k-1} = \hat{\boldsymbol{x}}_{k-1|k-1} - \left(\sqrt{(n+\lambda)\boldsymbol{P}_{k-1|k-1}}\right)_i, \end{cases} \tag{35}$$

where $i = 1, \ldots, n$ and the last term in the second and third expressions is the ith column (or row) of matrix square root of $(n+\lambda)\boldsymbol{P}_{k-1|k-1}$. In Eq. (35), n is the number of system states and λ will be introduced shortly. Then, each sigma point is propagated through the process model:

$$\hat{\boldsymbol{x}}^i_{k|k-1} = \boldsymbol{f}(\boldsymbol{\chi}^i_{k-1|k-1}, \boldsymbol{u}_{k-1}). \tag{36}$$

The predicted state estimate and the estimation error covariance are then given by:

$$\hat{\boldsymbol{x}}_{k|k-1} = \sum_{i=0}^{2n} W_i^{(m)} \hat{\boldsymbol{x}}^i_{k|k-1}, \tag{37}$$

$$\boldsymbol{P}_{k|k-1} = \sum_{i=0}^{2n} W_i^{(c)} (\hat{\boldsymbol{x}}^i_{k|k-1} - \hat{\boldsymbol{x}}_{k|k-1})(\hat{\boldsymbol{x}}^i_{k|k-1} - \hat{\boldsymbol{x}}_{k|k-1})^T, \tag{38}$$

where $W_i^{(m)}$ and $W_i^{(c)}$ are given by:

$$W_0^{(m)} = \frac{\lambda}{n+\lambda},$$
$$W_0^{(c)} = \frac{\lambda}{n+\lambda}(1-\alpha^2+\beta),$$
$$W_i^{(m)} = W_i^{(c)} = \frac{1}{2(n+\lambda)},$$

where $\lambda = \alpha^2(n+\kappa) - n$ is a scaling parameter in unscented transformation, $0 < \alpha < 1$ determines the spread of sigma point and κ is another free parameter either set to or $3-n$ [33]. Finally, β is a parameter to incorporate additional knowledge of distribution of the states (for Gaussian distribution $\beta = 2$) [33]. A similar procedure is adopted to calculate the measurement and its error covariance:

$$\begin{cases} \boldsymbol{\chi}^0_{k|k-1} = \hat{\boldsymbol{x}}_{k|k-1}, \\ \boldsymbol{\chi}^i_{k|k-1} = \hat{\boldsymbol{x}}_{k|k-1} + \left(\sqrt{(n+\lambda)\boldsymbol{P}_{k|k-1}}\right)_i, \\ \boldsymbol{\chi}^{i+n}_{k|k-1} = \hat{\boldsymbol{x}}_{k|k-1} - \left(\sqrt{(n+\lambda)\boldsymbol{P}_{k|k-1}}\right)_i, \end{cases} \tag{39}$$

$$\hat{\boldsymbol{y}}^i_k = \boldsymbol{H}\boldsymbol{\chi}^i_{k|k-1}, \tag{40}$$

$$\hat{\boldsymbol{y}}_k = \sum_{i=0}^{2n} W_i^{(m)} \hat{\boldsymbol{y}}^i_k, \tag{41}$$

$$\boldsymbol{P}^y_k = \sum_{i=0}^{2n} W_i^{(c)} (\hat{\boldsymbol{y}}^i_k - \hat{\boldsymbol{y}}_k)(\hat{\boldsymbol{y}}^i_k - \hat{\boldsymbol{y}}_k)^T + \boldsymbol{R}^*_k, \tag{42}$$

$$\boldsymbol{P}^{xy}_k = \sum_{i=0}^{2n} W_i^{(c)} (\hat{\boldsymbol{x}}^i_{k|k-1} - \hat{\boldsymbol{x}}_{k|k-1})(\hat{\boldsymbol{y}}^i_k - \hat{\boldsymbol{y}}_k)^T. \tag{43}$$

Once the measurements are available, the update equations are:

$$\boldsymbol{K}_k = \boldsymbol{P}^{xy}_k (\boldsymbol{P}^y_k)^{-1}, \tag{44}$$

$$\hat{\boldsymbol{x}}_{k|k} = \hat{\boldsymbol{x}}_{k|k-1} + \boldsymbol{K}_k(\boldsymbol{y}_k - \hat{\boldsymbol{y}}_k), \tag{45}$$

$$\boldsymbol{P}_{k|k} = \boldsymbol{P}_{k|k-1} - \boldsymbol{K}_k \boldsymbol{P}^y_k \boldsymbol{K}^T_k. \tag{46}$$

In the next section, a case study will be developed to evaluate the performance of our proposed approach.

Table 2. Characteristics of MUAV case study (partially from [35]).

Parameter	Value
UAV mass	4.34 kg
UAV moments of inertia	diag(0.0820, 0.0845, 0.1377) kg.m^2
Distance from a motor to UAV geometric center	0.33 m
Link(s) mass	0.20 kg
Link(s) length	0.20 m

5. Case Study, Simulation Results and Discussion

In this section, a MUAV consisting of a quadcopter equipped with a 2-DoF Revolute–Revolute robotic manipulator, confined to $X_B - Z_B$ plane of F_B is considered, please see Fig. 1. Mass properties of the MUAV and its geometric characteristics are given in Table 2. It is important to note that the links described above are identical. Also, the process noise covariance is assumed to be a constant diagonal matrix:

$$\begin{cases} Q^*(i,j) = 10^{-5} & \text{for } i = j = 9, 10, 11, \\ Q^*(i,j) = 10^{-6} & \text{for } i = j = 12, 13, 14, 15, 16, \\ 0 & \text{elsewhere}, \end{cases}$$

where $Q^*(i,j)$ is the ith row and jth column of $\boldsymbol{Q}^*$. Also, the measurement noise covariance is given by:

$$\begin{cases} R^*(i,j) = 10^{-3} & \text{for } i = j = 1, 2, 3, 4, \\ R^*(i,j) = 10^{-4} & \text{for } i = j = 5, 6, \\ 0 & \text{elsewhere}. \end{cases}$$

The values of translational elements of $\boldsymbol{Q}^*$ for our vehicle are close to those in Ref. 36 and the remaining elements are adapted accordingly. Regarding the measurement noise covariance, the values for translational elements are associated with accuracy of a few centimeters whereas measurement of the rotational element ψ complies with a few degrees accuracy. Similarly, measurement of robotic manipulator joint variables complies with degree-level accuracy. Also, initial conditions of the MUAV and the reference signal were considered as:

$$\boldsymbol{x}_{\text{MUAV}}(0) = \begin{bmatrix} 0.5\,\text{m} \\ -0.5\,\text{m} \\ 1\,\text{m} \\ 3\,\text{deg} \\ 0\,\text{deg} \\ 5\,\text{deg} \\ 0\,\text{deg} \\ 55\,\text{deg} \\ \boldsymbol{0}_{1\times 8} \end{bmatrix}, \quad \boldsymbol{x}^*_{\text{MUAV}}(0) = \begin{bmatrix} 0\,\text{m} \\ 0\,\text{m} \\ 2\,\text{m} \\ 0\,\text{deg} \\ 0\,\text{deg} \\ 0\,\text{deg} \\ 0\,\text{deg} \\ 90\,\text{deg} \\ \boldsymbol{0}_{1\times 8} \end{bmatrix}.$$

The MATLAB-based simulations were carried out on Intel® Core™–i5 3.2 GHz processor based computer with 8.00 GB RAM. For the described case study, simulations were carried out and obtained results are shown in Figs. 2 and 3, respectively. As it can be seen from Figs. 2 and 3, the proposed scheme has successfully accomplished UKF-based state estimation along with LQR–I control of a case study MUAV. In particular, state estimation of the MUAV position vector, i.e. X, Y, Z, has been achieved with centimeter-level accuracy. Also, the UKF-based algorithm has resulted in sub-degree state estimation of MUAV attitude, i.e. φ, θ, ψ channels. Similarly, sub-degree estimation of manipulator joint variables has been achieved. As it can be seen from Fig. 3,

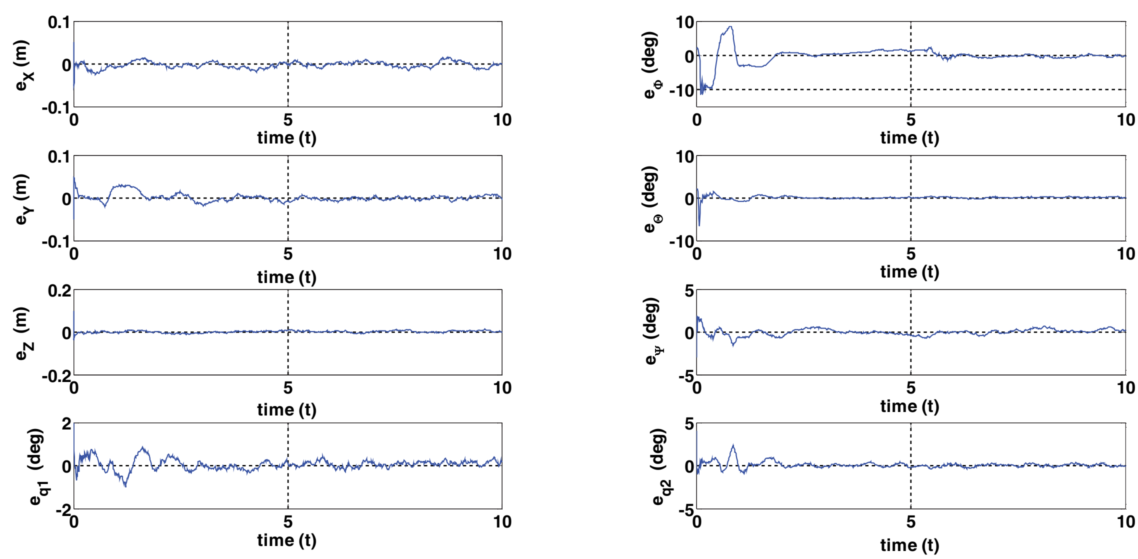

Fig. 2. UKF-based state estimation error of a case study MUAV.

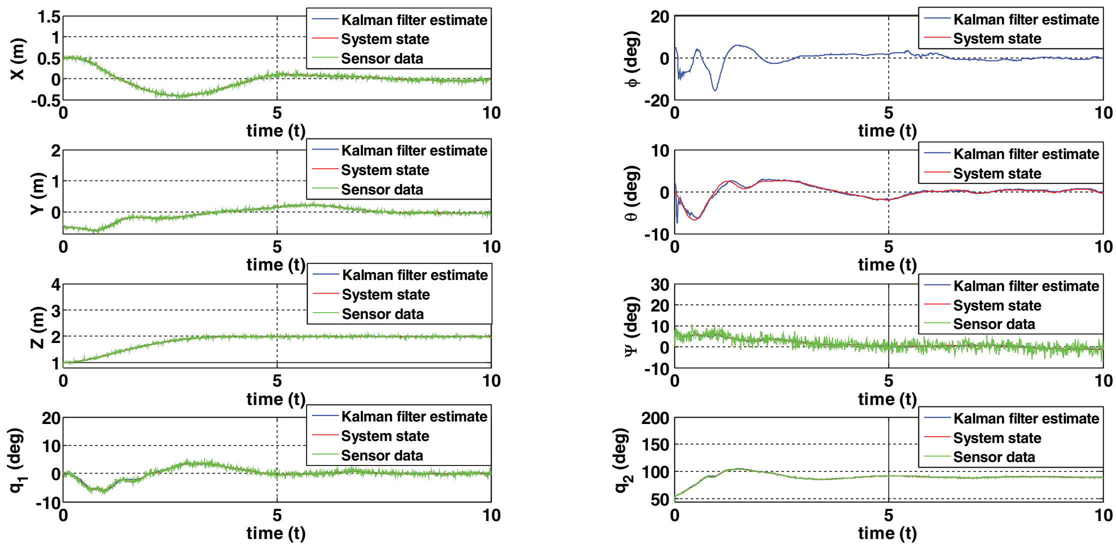

Fig. 3. UKF-based LQR-I control of a case study MUAV.

the LQR–I scheme can successfully control the MUAV such that position and three Euler angles of the quadcopter along with manipulator joint variables simultaneously converge to their desired reference value. In particular, position vector of the quadcopter has converged to its desired value with accuracies better than a few degrees in all three channels. Also, attitude of the UAV and manipulator joint variables have converged to their reference values with accuracy better than 2 degrees and 1 degree, respectively. Finally, it is important to note that complementing the LQR scheme with integral action has successfully resulted in elimination of the steady state error, commonly reported in LQR control applications [10].

6. Conclusions and Future Directions

In this paper, dynamic modeling, control and state estimation of an MUAV was examined. Regarding the control approach, it was shown that LQR controller complemented by integral actin can simultaneously control the UAV and its manipulator, i.e. the whole MUAV, and bring all the states to their desired references. The integral action was proved effective to eliminate the steady-state error observed in previous works.

Regarding state estimation, it was observed that our proposed UKF-based scheme can successfully achieve precise state estimation of an MUAV. However, we consider the computational complexity of UKF to become a bottleneck in actual onboard implementation for autonomous MUAV flight. In order to remedy that difficulty, we intend to examine two possible solutions. In the first approach, we will examine substitution of computationally–expensive Singular Value Decomposition used to obtain the matrix square root in UKF state estimation with Cholesky decomposition. In that manner, we expect to relatively relax our computational requirements, at the expense of a possibly less-stable solution. In the second approach, we will examine less computationally–expensive variants of unscented transformations which can be potentially employed to reduce the computational requirements of the current scheme, yet possibly rustling in relatively less-accurate state estimation.

Acknowledgment

This research was financially sponsored through a Discovery Grant No. # 203060-12 from the Natural Sciences and Engineering Research Council of Canada, NSERC.

References

[1] F. G. Costa, J. Ueyama, T. Braun, G. Pessin, F. S. Osório and P. A. Vargas, The use of unmanned aerial vehicles and wireless sensor network in agricultural applications, in *Proc. 2012 IEEE Int. Geoscience and Remote Sensing Symp. (IGARSS)*, (Munich, Germany, 2012), pp. 5045–5048.

[2] D. W. Casbeer, D. B. Kingston, R. W. Beard and T. W. McLain, Cooperative forest fire surveillance using a team of small unmanned air vehicles, *Int. J. Syst. Sci.* **37**(6) (2006) 351–360.

[3] H. A. F. Almurib, P. T. Nathan and T. N. Kumar, Control and path planning of quadrotor aerial vehicles for search and rescue, in *Proc. IEEE SICE Annual Conf. (SICE)* (Tokyo, Japan, 2011), pp. 700–705.

[4] H. Li, B. Wang, L. Liu, G. Tian, T. Zheng and J. Zhang, The design and application of SmartCopter: An unmanned helicopter based robot for transmission line inspection, in *Proc. IEEE Chinese Automation Congress (CAC)* (Changsha, China, 2013), pp. 697–702.

[5] R. W. Beard, T. W. McLain, D. B. Nelson, D. Kingston and D. Johanson, Decentralized cooperative aerial surveillance using fixed–wing miniature UAVs, *Proc. IEEE* **94**(7) (2006) 1306–1324.

[6] N. Michael, J. Fink and V. Kumar, Cooperative manipulation and transportation with aerial robots, *Autonomous Robots*, **30**(1) (2011) 73–86.

[7] D. Mellinger, Q. Lindsey, M. Shomin and V. Kumar, Design, modeling, estimation and control for aerial grasping and manipulation, in *Proc. IEEE/RSJ Int. Conf. Intelligent Robots and Systems (IROS)* (San Francisco, USA, 2011) pp. 2668–2673.

[8] J. Thomas, G. Loianno, K. Sreenath and V. Kumar, Toward image based visual servoing for aerial grasping and perching, in *Proc. IEEE Int. Conf. Robotics and Automation (ICRA)* (Hong Kong, China, 2014) pp. 2113–2118.

[9] G. Gioioso, M. Ryll, D. Prattichizzo, H. H. Bulthoff and A. Franchi, Turning a near–hovering controlled quadrotor into a 3D force effector, in *Proc. IEEE Int. Conf. Robotics and Automation (ICRA)* (Hong Kong, China, 2014) pp. 6278–6284.

[10] H. Bonyan Khamseh and F. Janabi–Sharifi, Modeling and control of a manipulating unmanned aerial vehicle, in *Proc. Canadian Society for Mechanical Engineering (CSME) International Congress*, June 2016, Kelowna, BC, Canada.

[11] V. Lipiello and F. Ruggiero, Cartesian impedance control of a uav with a robotic arm, in *Proc. 10th IFAC Symp. Robot Control* (Dubrovnik, Croatia, 2012), pp. 704–709.

[12] H. Yang and D. Lee, Dynamics and control of quadrotor with robotic manipulator, in *Proc. IEEE International Conference on Robotics and Automation* (Hong Kong, 2014), pp. 5544–5549.

[13] S. Kannan, M. A. Olivares-Mendez and H. Voos, Modeling and control of aerial manipulation vehicle with visual sensor, in *Proc. Research, Education and Development of Unmanned Aerial Systems* (Compiegne, France, 2013), pp. 303–309.

[14] A. Khalifa, M. Fanni, A. Ramadan and A. Abo–Ismail, Modeling and control of a new quadrotor manipulation system, in *Proc. First Int. Conf. Innovative Engineering Systems (ICIES)* (Alexandria, Egypt, 2012), pp. 109–114.

[15] G. Garimella and M. Kobilarov, Towards Model–predictive Control for Aerial Pick-and-Place, in *Proc. IEEE Int. Conf. Robotics and Automation (ICRA)* (Seattle, USA, 2015), pp. 4692–4697.

[16] B. Yang, Y. He, J. Han and G. Liu, Rotor-flying manipulator: Modeling, analysis, and control, *Mathematical Problems in Engineering* **2014** (2014) Article ID 492965 (13 pages), doi: 10.1155/2014/492965, https://www.hindawi.com/journals/mpe/2014/492965/cta/

[17] M. Orsag, C. M. Korpela, S. Bogdan and P. Y. Oh, Hybrid adaptive control for aerial manipulation, *J. Intell. Robotic Syst.* **73**(1) (2014) 693–707.

[18] M. Orsag, C. Korpela, M. Pekala and P. Oh, Stability control in aerial manipulation, in *Proc. American Control Conf. (ACC)* (Washington, USA, 2013), pp. 5581–5586.

[19] G. Heredia, A. E. Jimenez-Cano, I. Sanchez, D. Llorente, V. Vega, J. Braga, J. A. Acosta and A. Ollero, Control of a multirotor outdoor aerial manipulator, in *Proc. IEEE/RSJ Int. Conf. Intell. Robots Syst. (IROS)* (Chicago, USA, 2014), pp. 3417–3422.

[20] A. Y. Mersha, S. Stramigioli and R. Carloni, Exploiting the dynamics of a robotic manipulator for control of UAVs, in *Proc. IEEE Int. Conf. Robotics and Automation (ICRA)* (Hong Kong, China, 2014), pp. 1741–1746.

[21] M. Kobilarov, Nonlinear trajectory control of multi–body aerial manipulators, *J. Intell. Robotic Syst.* **73**(1) (2014) 679–692.

[22] I. D. Cowling, O. A. Yakimenko, J. F. Whidborne and A. K. Cooke, A prototype of an autonomous controller for a quadrotor UAV, in *Proc. European Control Conf. (ECC)* (Kos, Greece, 2007), pp. 4001–4008.

[23] M. Belkheiri, A. Rabhi, A. E. Hajjaji and C. Pegard, Different linearization control techniques for a quadrotor system, in *Proc. 2nd Int. Conf. Communications, Computing and Control Applications (CCCA)*, (Marseilles, France, 2012), pp. 1–6.

[24] E. Reyes-Valeria, R. Enriquez-Caldera, S. Camacho-Lara and J. Guichard, LQR control for a quadrotor using unit quaternions: Modeling and simulation, in *Proc. Int. Conf. Electronics, Comm. and Computing*, (Cholula, Mexico, 2013), pp. 172–178.

[25] S. Julier, J. Uhlmann and H. F. Durrant-Whyte, A new method for the nonlinear transformation of means and covariances in filters and estimators, *IEEE Trans. Automatic Control.* **45**(3) (2000) 477–482.

[26] J. Julier Simon and J. K. Uhlmann, A new extension of the Kalman filter to nonlinear systems, in *Proc. AeroSense* (Orlando, FL, 1997), pp. 182–193.

[27] A. Giannitrapani, N. Ceccarelli, F. Scortecci and A. Garulli, Comparison of EKF and UKF for spacecraft localization via angle measurements, *IEEE Trans. Aerospace and Electronic Syst.* **47**(1) (2011) 75–84.

[28] H. G. De Marina, F. J. Pereda, J. M. Giron-Sierra and F. Espinosa, UAV attitude estimation using unscented Kalman filter and TRIAD, *IEEE Trans. Industrial Electron.* **59**(11) (2012) 4465–4474.

[29] B. Siciliano, L. Sciavicco, L. Villani and G. Oriolo, *Robotics: Modelling, Planning and Control* (Springer Science & Business Media, 2010).

[30] D. E. Kirk *Optimal Control Theory: An Introduction* (Mineola, NY, Dover Publications Inc., 1970).

[31] Y. Bar-Shalom, X. R. Li and T. Kirubarajan, *Estimation with Applications to Tracking and Navigation* (John Wiley and Sons, 2001).

[32] A. Assa and F. Janabi-Sharifi, A Kalman filter-based framework for enhanced sensor fusion, *IEEE Sensors J.* **15**(6) (2015) 3281–3292.

[33] S. Kolas, B. A. Foss and T. S. Schei, Constrained nonlinear state estimation based on the UKF approach, *Comput. Chem. Eng.* **33**(8) (2009) 1386–1401.

[34] E. A. Wan and R. van der Merwe, The unscented Kalman filter for nonlinear estimation, in *Proc. IEEE Adaptive Systems for Signal Processing, Communications and Control Symp.* (Lake Louise, Alta, 2000), pp. 153–158.

[35] P. Pounds, R. Mahony and P. Corke, Modelling and control of a large quadrotor robot, *Control Eng. Prac.* **18**(7) (2010) 691–699.

[36] M. H. Amoozgar, A. Chamseddine and Y. Zhang, Experimental test of a two-stage Kalman filter for actuator fault detection and diagnosis of an unmanned quadrotor helicopter, *J. Intell. Robotic Syst.* **70**(N1) (2013) 107–117.

Hossein Bonyan Khamseh received his B.Sc. and M.Sc. in Aerospace Engineering from Amirkabir University and Shahid Beheshti University in 2008 and 2010, respectively. He served as co-principal investigator of a university-funded project at Shahid Beheshti University to investigate the effects of ground segment location on responsiveness of low-earth-orbit satellites. Afterwards, he worked as a systems engineer in Amirkabir University of Technology Satellite (AUTSAT) project 2011–2012. From 2012 to 2014, he was with the Electrical Engineering Department of Universidade Federal de Minas Gerais, Brazil, where he worked on path planning of fixed-wing UAVs in formation flight. He is currently pursuing his Ph.D. degree at Mechanical and Industrial Engineering Department of Ryerson University, Toronto, Canada. His current research interests include aerial manipulation, aerial robotics, estimation, control, and visual servoing. He has authored and co-authored more than 20 conference and journal papers and a book chapter. He has also served a number of roles including more than 10 conference/journal reviewer and co-chair positions, invited speaker, and instructor in various capacities.

Farrokh Janabi-Sharifi (S'91–M'95–SM'02) is a Professor of Mechanical-Industrial Engineering and the Director of Robotics, Mechatronics and Manufacturing Automation Laboratory (RMAL) at Ryerson University, Toronto, Canada. He received the Ph.D. degree in Electrical and Computer Engineering from the University of Waterloo, Canada in 1995. He was NSERC postdoctoral fellow and instructor in the Center for Intelligent Machines and Department of Electrical-Computer Engineering of McGill University (1995–1997). His research interests span over optomechatronic systems with the focus on image-guided control and planning of robots. He has been a visiting professor in KAIST, Taejon, Korea; IRISA-INRIA, Rennes, France; and TUM, Munich, Germany. He has also been an Organizer and/or Co-organizer of several international conferences on optomechatronic systems control. He was the General Chair of 2010 International Symposium on Optomechatronic Technologies, Toronto, Canada. He currently serves as the Associate Editor of several journals including International Journal of Optomechatronics.